Hindawi
Adsorption Science & Technology
Volume 2022, Article ID 1924117, 14 pages
https://doi.org/10.1155/2022/1924117

Research Article

Adsorption of Phenol onto Aluminum Oxide Nanoparticles: Performance Evaluation, Mechanism Exploration, and Principal Component Analysis (PCA) of Thermodynamics

Safwat M. Safwat,[1] **Nouran Y. Mohamed**,[2] **Mohamed N. A. Meshref**,[3,4] **and Abdelsalam Elawwad**[1]

[1]*Sanitary & Environmental Engineering Division, Public Works Department, Faculty of Engineering, Cairo University, Giza 12316, Egypt*
[2]*Housing & Building National Research Center, Giza, Egypt*
[3]*Public Works Department, Faculty of Engineering, Ain Shams University, 1 El Sarayat St., Abbassia, Cairo 11517, Egypt*
[4]*University of Alberta, Edmonton, Alberta, Canada*

Correspondence should be addressed to Abdelsalam Elawwad; elawwad@cu.edu.eg

Received 30 December 2021; Revised 22 February 2022; Accepted 4 March 2022; Published 4 April 2022

Academic Editor: Senthil Kumar Ponnusamy

The removal of phenolic compounds from aqueous solutions using novel adsorption techniques becomes a key research item. Of those, nanoparticles in particular, the low-cost and the high-strength aluminum oxide nanoparticles showed promising results in pollutant uptake and increase in the adsorption efficiency. This study examined various physicochemical process parameters such as temperature, pH, initial phenol concentration, and adsorbent doses, in addition to the impact of those parameters on the adsorption removal mechanism of phenol. The results highlighted that aluminum oxide nanoparticles successfully exhibited superior phenol removal from an aqueous solution in addition to a high potential regeneration of the consumed nanoparticles by HCl. For the adsorbent mass of 0.5 g, phenol adsorption uptake reached 92%. Kinetic studies performed using several models demonstrated the data best fitting with a pseudo-second-order kinetic model. Examining equilibrium studies of various isotherms, the adsorption data of phenol into aluminum oxide nanoparticles was confirmed to be controlled by film diffusion and best represented by the Langmuir isotherm. The maximum capacity of adsorption was 16.97 mg/g. For thermodynamics studies, the results indicated that the adsorption process can vary between endothermic and exothermic reactions. Such relative differences in heat generation and spontaneity in adsorption processes were demonstrated and confirmed by principal component analysis (PCA). This evidence is key for future investigations for the efficiency of adsorption conditions concerning the contaminant type and adsorbate compounds.

1. Introduction

Phenol is a common aromatic hydrocarbon, which is toxic and very soluble in water [1]. It exists in high concentrations in various types of wastewater, such as pesticide, chemical manufacturing, pulp, plastic, textile, coke manufacturing, dyes, and resin-manufacturing effluents [2]. Its concentration in effluents can range from 1 mg/L to several hundred milligrams per liter [3]. Due to its deployment as raw material or intermediate compounds or being generated as a final product, large quantities of phenolic compound effluent possess issues [4]. Phenol can cause severe health problems to the skin, eyes, lungs, liver, kidneys, and central nervous system [2]. Phenol is also toxic to plants and aquatic life [3]. The phenol concentration in wastewater should not surpass 1 mg/L according to the Environmental Protection Agency [2]. As a result, wastewater containing phenol should be treated before discharging it into the environment. Several

technologies can be used to reduce the concentration of phenol in wastewater, such as chemical oxidation, electrochemical techniques, membranes, and biological treatment methods. However, chemical techniques are expensive and can produce harmful byproducts [5, 6]. Nonetheless, the biodegradation of phenol using biological processes is still a challenge because it can inhibit microorganisms at high concentrations [7, 8]. Alternatively, the removal of phenol using membrane technologies is associated with a very high cost.

Adsorption is one of the technologies that can remove phenol from wastewater by transferring it from the liquid phase to a solid surface [9–11]. The development of various adsorption technologies in comparison to other chemical technologies can be attributed to their low cost and their simplicity. It is also insensitive of toxic substances [12]. Additionally, adsorption proved to be successful in the removal of both inorganic and organic pollutants from wastewater [13–16] and highly efficient at low concentrations of contaminants [4] with a minimal byproducts. Various types of adsorbents have been examined in the removal of different pollutants [17, 18]. Moreover, coupling nanotechnology with adsorption has been found to be very efficient. Nanoparticles have a large surface area and can be supported on various materials [19]. Several types of nanoparticles have been examined in the uptake of pollutants from aqueous solutions [20]. For instance, carbon nanotubes have been employed in the removal of heavy metals [21]. Iron oxide nanoparticles and copper oxide nanoparticles have been used in the removal of arsenic from wastewater [22, 23]. Similarly, the removal of various contaminants from aqueous solution such as arsenate, chromium, and mercury was attained using zirconium-based nanoparticles [24], carbon nano-onions [25], and nano-titanium dioxide [26], respectively.

Aluminum oxide nanoparticles are among the first inorganic nanoparticles to be examined as an adsorbent material. This is due to their high efficiency in pollutant uptake and their high strength and low cost [27]. The main disadvantage is the separation process when applied on a full scale. A previous study has shown that aluminum oxide nanoparticles were able to remove orange G and their adsorption capacity was 93.3 mg/g [27]. Another study used aluminum oxide nanoparticles in the removal of cadmium and lead, and the adsorption capacities were 78 and 217 mg/g, respectively [28]. A third study showed that thiophenes can be adsorbed using aluminum oxide nanoparticles [29]. Another study examined the ability of aluminum oxide nanoparticles to remove methylene blue, and the maximum capacity of adsorption was $2.5 * 10^{\times 5}$ mol/g [30]. Fluoride was also removed using aluminum oxide nanoparticles, and the adsorption capacity reached about 65 mg/g [31]. In the same matter, other studies have examined the removal of phenolic compounds using various nanoparticles. For example, Liu et al. examined the ability of hierarchical micronanoporous carbon material in the removal of phenol [32]. In another study by Kim et al. , nanostructured silicas functionalized with phenyl groups were able to uptake bisphenol from an aqueous solution [33].

While aluminum oxide powder was previously examined to remove phenol from aqueous solution and showed good results in the adsorption process [34], it can be hypothesized that applying aluminum oxide material in a nanoscale can improve the adsorptive removal efficiency of the pollutants. Given these facts and the apparent research gaps, examining the ability of aluminum oxide in the form of nanoparticles as an adsorbent [35, 36] is crucial. Moreover, phenol can cause severe environmental and health problems if it is not removed from wastewater. To the best of the authors' knowledge, the phenol removal from an aqueous solution using aluminum oxide nanoparticles has not yet been studied. The overall objective is to study the capacity of aluminum oxide nanoparticles to remove phenol from an aqueous solution in different experimental conditions. The manuscript also presents detailed information and investigations regarding the adsorption kinetics, adsorption capacity, equilibrium, thermodynamics, and isotherm interpretation in addition to the regeneration and desorption potential of the adsorbent.

2. Materials and Methods

2.1. Preparation of Aluminum Oxide Nanoparticles. The preparation of aluminum oxide nanoparticles was performed using the c-precipitation technique with aluminum sulfate and sodium hydroxide precursors as described elsewhere [37]. 0.1 M of aluminum sulfate was dissolved in a distilled water, and the solution was then preserved under constant stirring for one hour. After the complete dissolution of the aluminum sulfate, 0.2 M of sodium hydroxide solution was added. The white creamy solution was left to settle overnight, and then, the supernatant was carefully discarded. The precipitate was washed several times using distilled water and then was dried overnight at 80°C. Complete conversion of aluminum hydroxide into alumina during drying was attained. The Brunauer–Emmett–Teller (BET) surface area was determined by N_2 adsorption/desorption. The X-ray diffraction (XRD) pattern was obtained for aluminum oxide nanoparticles using X'Pert Pro with a monochromator with Cu radiation. Measurements were performed at 45 kV and 35 mA. The reflection peaks were obtained using a 0.03°/s scanning velocity at 2θ from 10° to 70°.

2.2. Adsorption Experiments. Batch experiments of adsorption were conducted at 30°C ± 2°C. Several initial concentrations of phenol ranging from 10 mg/L to 1000 mg/L and various doses (0.1 g–0.5 g) of aluminum oxide nanoparticles ranging were examined. The experiments were performed using flasks that contained the phenol aqueous solution. These were shaken at various speeds ranging from 50 rpm to 300 rpm. The initial pH was adjusted using either 0.1 N of sodium hydroxide or 0.1 N of dilute hydrochloric acid. After the adsorption process, the samples were filtered using filter papers. The phenol concentrations were determined using the digital photometer NANOCOLOR® 500 D using the procedures described in the standard methods for the examination of water and wastewater [38]. To verify the stability of phenol during experiments, control experiments were conducted.

2.3. Kinetics, Equilibrium, and Thermodynamics. Several modeling techniques can be used to predict the efficiency of the adsorption process [39]. Adsorption experiments were conducted at different contact times (5–120 min) to perform kinetic studies. The thermodynamic experiments were performed at four different temperatures ranging from 30°C to 60°C while the equilibrium models were studied at the equilibrium contact time (2 h). To perform the kinetic calculations, the following linear equations were used for the PFO and PSO kinetic models, the Elovich model, intraparticle diffusion model, and Boyd model [40]:

$$\begin{gathered} q_t = (C_0 - C_t)\frac{V}{W}, \\ q_e = (C_0 - C_e)\frac{V}{W}, \\ \ln\ (q_e - q_t) = \ln\ (q_e) - k_1 t, \\ \frac{t}{q_t} = \frac{1}{q_e}t + \frac{1}{k_2 q_e^2}, \\ q_t = \frac{1}{\beta}\ln\ (\alpha\beta) + \frac{1}{\beta}\ln\ (t), \\ qt = k_p t^{0.5} + C, \end{gathered} \tag{1}$$

$$Bt = -0.4977 - \ln\left(1 - \frac{q_t}{q_e}\right), \tag{2}$$

where the initial concentration of phenol is C_0, the concentration of phenol at time t is C_t, and the concentration of phenol at equilibrium is C_e. The volume of the aqueous solution is denoted by V, and the mass of the aluminum oxide nanoparticles is W, and the amount of phenol adsorbed per mass of aluminum oxide nanoparticles at equilibrium is denoted by q_e. In addition, t indicates the time, k_1 is the PFO rate constant, and k_2 is the PSO rate constant. Furthermore, α represents the initial rate constant, β indicates the desorption constant, and k_p denotes the intraparticle diffusion model rate constant. Finally, C is the constant associated with the boundary layer thickness and Bt represents a mathematical function of q_t/q_e.

The amount of adsorbed phenol onto aluminum oxide nanoparticles at equilibrium can be expressed using several adsorption isotherms. The following four isotherms (Langmuir, Freundlich, Dubinin-Radushkevich, and Temkin) have been used in equilibrium studies. The linear forms of these isotherms are stated as follows:

$$\begin{gathered} \frac{1}{q_e} = \left(\frac{1}{Q_{\max}K_L}\right)\frac{1}{C_e} + \frac{1}{Q_{\max}}, \\ \operatorname{Log} q_e = n \log\ C_e + \log\ K_F, \\ \ln\ q_e = -K_{DR}R^2T^2\ln^2\left(1 + \frac{1}{C_e}\right) + \ln\ q_{DR}, \\ q_e = B_1\ln\ K_T + B_1\ln\ C_e, \end{gathered} \tag{3}$$

where the maximum adsorption capacity is $Q_{\max}$. In addition, K_L denotes a constant linked to the affinity between phenol and nanoparticles, n is the Freundlich intensity parameter, and K_F is the Freundlich constant. Moreover, K_{DR} represents a constant linked to the sorption energy and q_{DR} denotes the adsorption capacity. Furthermore, R represents the gas constant, T is the temperature, and B_1 indicates the Temkin isotherm constant. Finally, K_T denotes the Temkin isotherm equilibrium binding constant. To calculate the parameters obtained from thermodynamic studies, the following equations were used:

$$\begin{gathered} K_C = \frac{C_{Ae}}{C_e}, \\ \Delta G^\circ = -RT\ln K_c, \\ \ln K_C = \frac{\Delta S^\circ}{R} - \frac{\Delta H^\circ}{RT}, \end{gathered} \tag{4}$$

where Kc is the constant of equilibrium and C_{Ae} denotes the amount of adsorbed phenol onto the nanoparticles per liter of solution at equilibrium. In addition, ΔG° is the Gibbs-free energy, ΔH° is the enthalpy, and ΔS° is the entropy.

Statistical analyses such as one-way analysis of variance (ANOVA) and Tukey pairwise comparisons in Minitab were performed to compare and determine the significant similarity and differences between different conditions and the characteristics of their samples. For any statistical differences, various key parameters and normality of the data were considered (i.e., analysis of data distribution was pre-examined for normality to decide the applicable test). To compare the significant differences in the values of the mean of the datasets, the p values were calculated with a significant level of 0.05 and considered significant at p values < 0.05. To evaluate the relationships and variations between the treatment conditions and verify their clustering and distinctions, multivariate analysis of variance such as principal component analysis (PCA) and cluster analysis were performed using Minitab [41]. Statistical tests on the significance of the similarities/differences of data might not be likely represented while using the same dataset in the same group; therefore, any differences in the replication of measurements in the same group between conditions were examined. All data were mean values of few replicates unless otherwise stated.

3. Results and Discussion

3.1. Characterization of Aluminum Oxide Nanoparticles. Figure 1(a) shows the aluminum oxide XRD spectra. The adsorbent is crystalline in nature due to the presence of peaks. The Brunauer–Emmett–Teller (BET) surface area was found to be 6.26 m^2/g, and this is consistent with Prabhakar and Samadder [42]. Fourier-transform infrared (FTIR) spectroscopy was performed for the aluminum oxide nanoparticles, as shown in Figure 1(b). The peaks observed at 615 and 636 are assigned to the aluminum oxide stretching. The peak at 1127 indicates the triply degenerate vibrational mode of the sulfate ion. The peaks at 1646 and 3526 are related to the bending and stretching vibration mode of

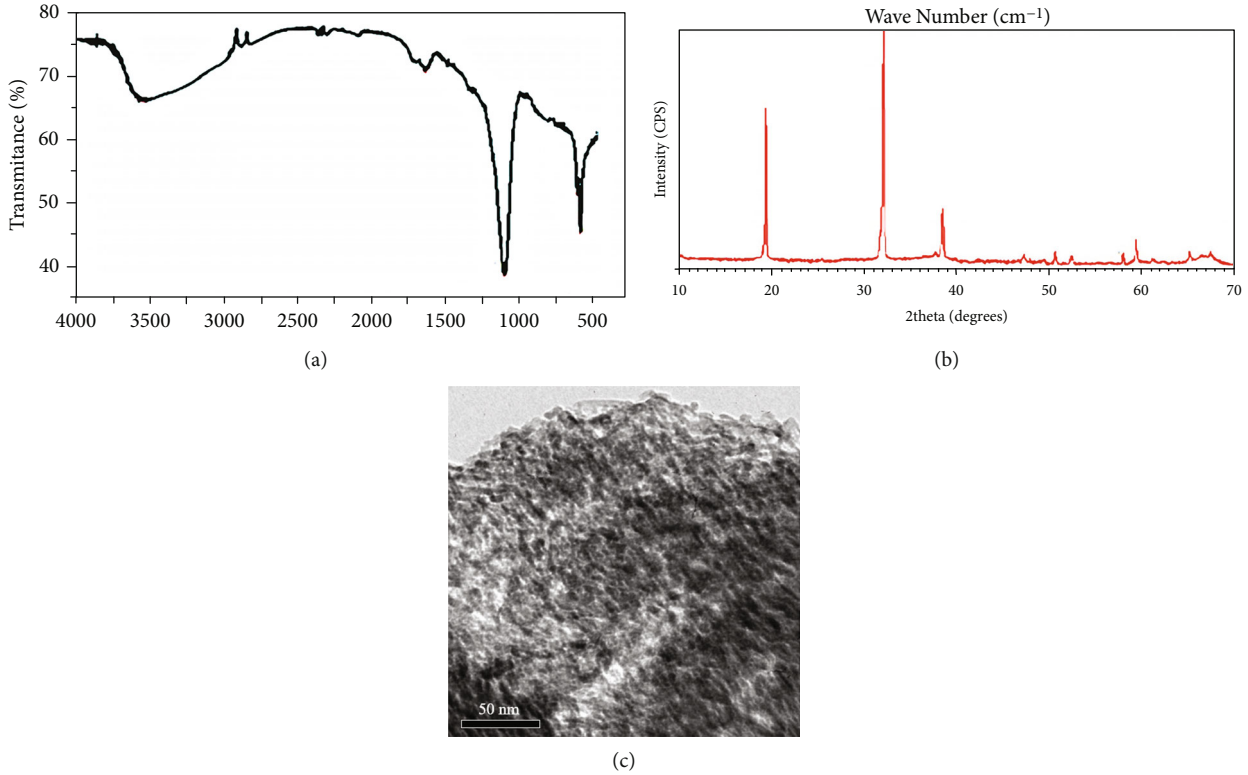

Figure 1: The characterization of the aluminum oxide nanoparticle adsorbent material using (a) the X-ray diffraction pattern, (b) Fourier-transform infrared spectroscopy, and (c) transmission electron microscopy image.

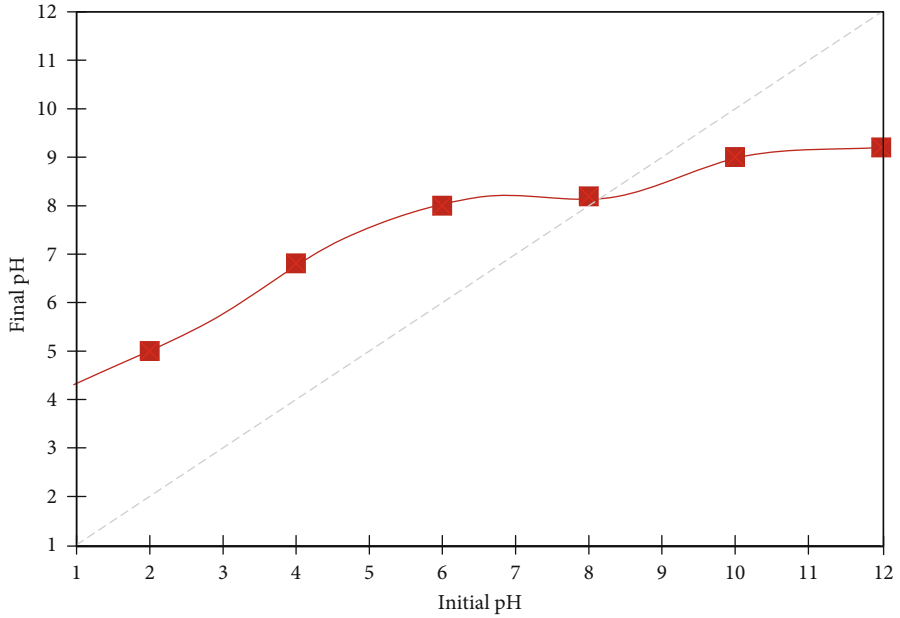

Figure 2: Plot of the pH drift method.

a water molecule [4]. The examination of the surface of the aluminum oxide nanoparticles was performed using a transmission electron microscope. Figure 1(c) reveals that all particles are well crystallized, and the size of the particles is in the nanorange.

As illustrated in Figure 2, the zero charge point (pH_{pzc}) was obtained using the pH drift method, as described elsewhere [43]. The pH of a solution is a critical parameter that impacts the adsorption of contaminants such as dyes and phenols. The solution pH can be a determinant level of the

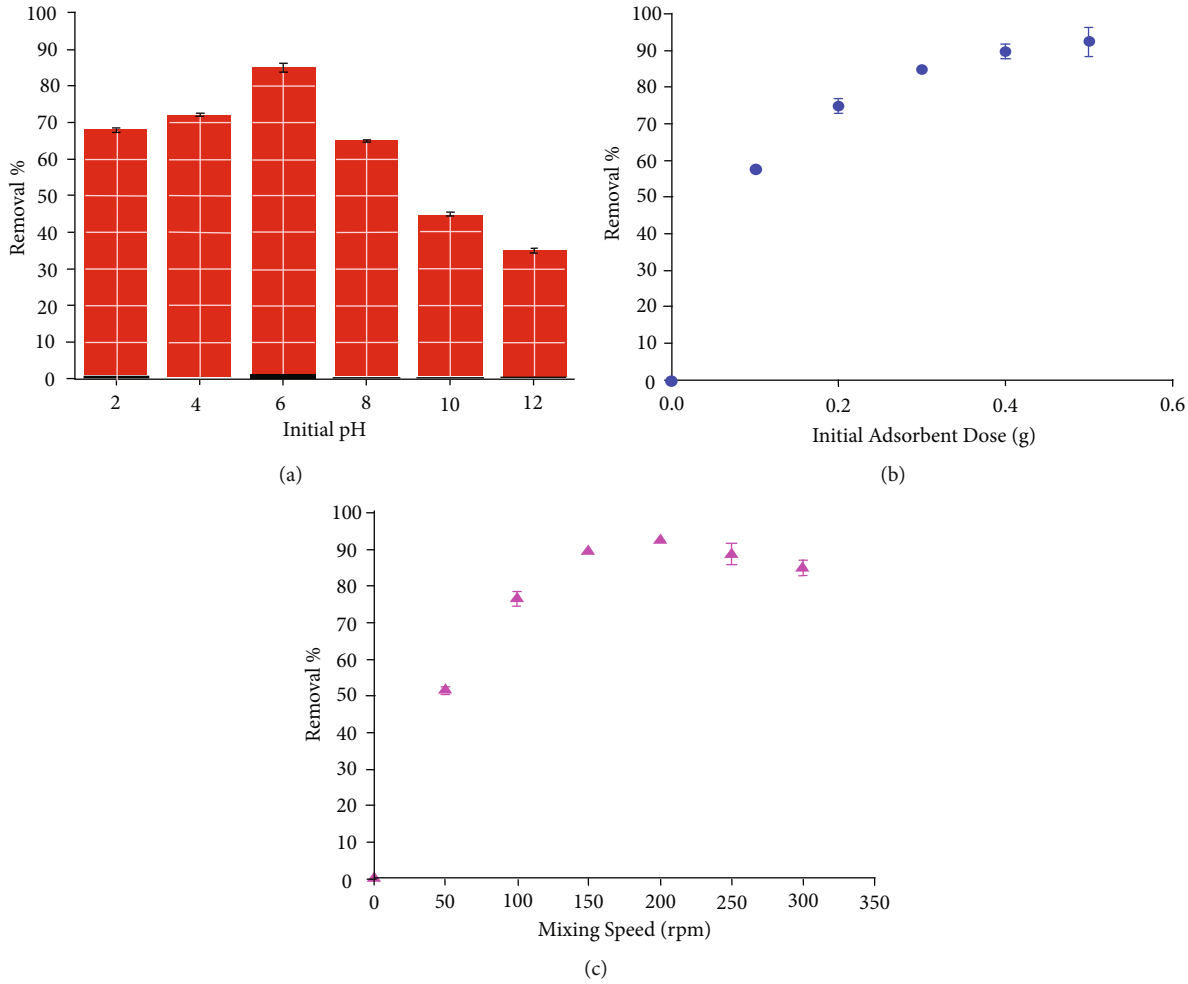

FIGURE 3: The removal efficiency of phenol at (a) various pH levels at an applied adsorbent dose = 0.5 g, initial phenol concentration = 100 mg/L, contact time = 2 h, and stirring speed = 200 rpm; (b) various adsorbent doses at an initial phenol concentration = 400 mg/L, pH = 6, contact time = 2 h, and stirring speed = 200 rpm; and (c) various stirring speeds at an initial phenol concentration = 400 mg/L, pH = 6, contact time = 2 h, and applied adsorbent dose = 0.5 g.

electrostatic and molecular' interaction between the adsorbent surface and the adsorbate owing to charge distribution on the material [44, 45]. Accordingly, the pH_{pzc} of aluminum oxide nanoparticles was determined at 8. This value is similar to what was reported in previous studies [30].

3.2. Influence of the Initial pH, Initial Adsorbent Dose, and Stirring Speed. Various effects of the experimental operating conditions were investigated as depicted in Figures 3(a)–3(c). The effect of the initial pH was investigated to demonstrate its impact on the adsorption process (Figure 3(a)) and the removal efficiency of phenol at various initial pH values (2, 4, 6, 8, 10, and 12). The results demonstrated that the best removal efficiency was obtained at a pH of 6 with 85% removal. At higher pH values, the removal efficiencies were lower than those obtained at lower pH values. This phenomenon could be related to the pH_{pzc} of aluminum oxide nanoparticles. At a pH of less than pH_{Pzc}, the adsorbent surface is positively charged. Phenol acts as a weak acid, as shown in equation (5) where $pK_a = 10$ [46]. The nanoparticle surface in an acidic solution is positively charged, while the equilibrium shifts to the left. Thus, phenol uptake happens due to the dipole-dipole interaction. The positively charged functional group of the nanoparticles interacts with the negatively charged hydroxyl group. At much lower pH (less than 6), additional protons exist, which compete for the adsorbent sites [47]. Furthermore, at high pH values, the equation shifts to the left. Due to the negative charges of the nanoparticle surface at high pH values, a repulsion force occurs, leading to a decrease in the removal efficiency.

$$C_6H_5OH + H_2O \leftrightarrows C_6H_5O^- + H_3O^+. \quad (5)$$

With regard to the initial adsorbent dose (Figure 3(b)), the effects of different adsorbent doses of aluminum oxide nanoparticles ranging from 0.1 g to 0.5 g were examined. The adsorption stages usually encompass an initial stage followed by a second stage. A high mass transfer driving force is expected by the high phenol concentration at the initial stages of the adsorption process. For adsorbent mass of 0.5 g, the phenol adsorption uptake reached to 92%. The

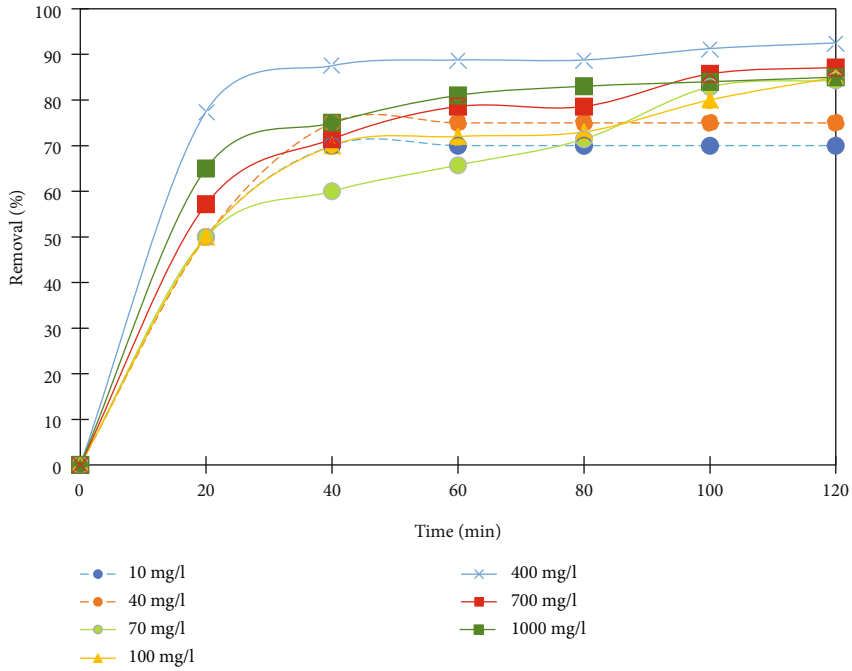

Figure 4: Removal efficiency of phenol at various initial concentrations at dose = 0.5 g, pH = 6, contact time = 2 h, and stirring speed = 200 rpm.

increase of the initial aluminum oxide concentration from 0.1 g to 0.3 g led to 30% increase in the removal efficiency. However, the maximum uptake reached a plateau above 0.5 g of adsorbent mass. It is worth noting that the available adsorption sites could increase with the increase of adsorbent doses that leads to a greater ability to adsorb phenol. This reflects the high dependence of the adsorption process on the initial concentration, and the increase in initial concentration could have a significant effect on the final equilibrium time [48, 49].

The effect of the stirring speed on the removal efficiency of phenol was determined (Figure 3(c)). The overall trend is the increase of the removal efficiency of phenol with the increase of stirring speed. However, when we applied various stirring speed range (50 rpm to 300 rpm), a plateau was observed with a slight decline above a stirring speed of 200 rpm. This phenomenon where the efficiency of the phenol removal had a cut off stirring speed at 200 rpm can be attributed to the available adsorption sites. The high stirring and mixing speeds are able to force the phenol to penetrate the micropores and reach more available adsorption sites. However, at a stirring speed of more than 200 rpm, the high speed caused shear forces that led to the desorption of phenol from the surface of the adsorbent and resulted in a decrease of the adsorption capacity (i.e., removal efficiency) [50]. It is worth remarking that the adsorbed molecules could also create repulsive forces during the later stage of adsorption which can be boosted at high stirring speed. The former fact indicates the major effect of stirring speed as a major factor in the determination of the mechanism of adsorption and adsorption rates [49].

3.3. Influence of the Initial Phenol Concentration and Contact Time. The adsorption kinetics is important for the selection of the optimum operating conditions for the full-scale adsorption processes [49]. Thus, the effects of the initial concentration of phenol and the contact time were investigated, as shown in Figure 4. The results showed that the removal efficiencies increased rapidly in the first 20 min and more than 50% of the removal was achieved for all concentrations. Subsequently, the removal efficiencies increased slowly until reaching equilibrium after 2 h. The maximum removal efficiency during the entire experiment duration was obtained at 400 mg/L at a removal efficiency level of 92.5%. The results revealed that the initial concentrations have a significant effect on the removal efficiencies of phenol. To grab a better understanding, at the low phenol concentrations (<400 mg/L), their removal efficiencies increased due to the high adsorption sites present in the aluminum oxide nanoparticles, which can accommodate these ranges of phenol concentrations. The combination of the large number of vacant and available adsorption sites with the high concentration of the adsorbate at the initial stage could provide a high driving force for adsorption at these moderate and small concentrations. On the other hand, at higher concentrations, the available sites of adsorbent are not adequate to accommodate higher concentrations, so the removal efficiencies decreased. Using this hypothesis, the number of available sites could also decrease with time while the adsorbate molecules start to compete for the remaining sites and the adsorbed molecules start to create repulsive forces during further adsorption. The kinetics section illustrated later can highlight these findings with respect to the adsorption rate and the potential of the fast adsorption

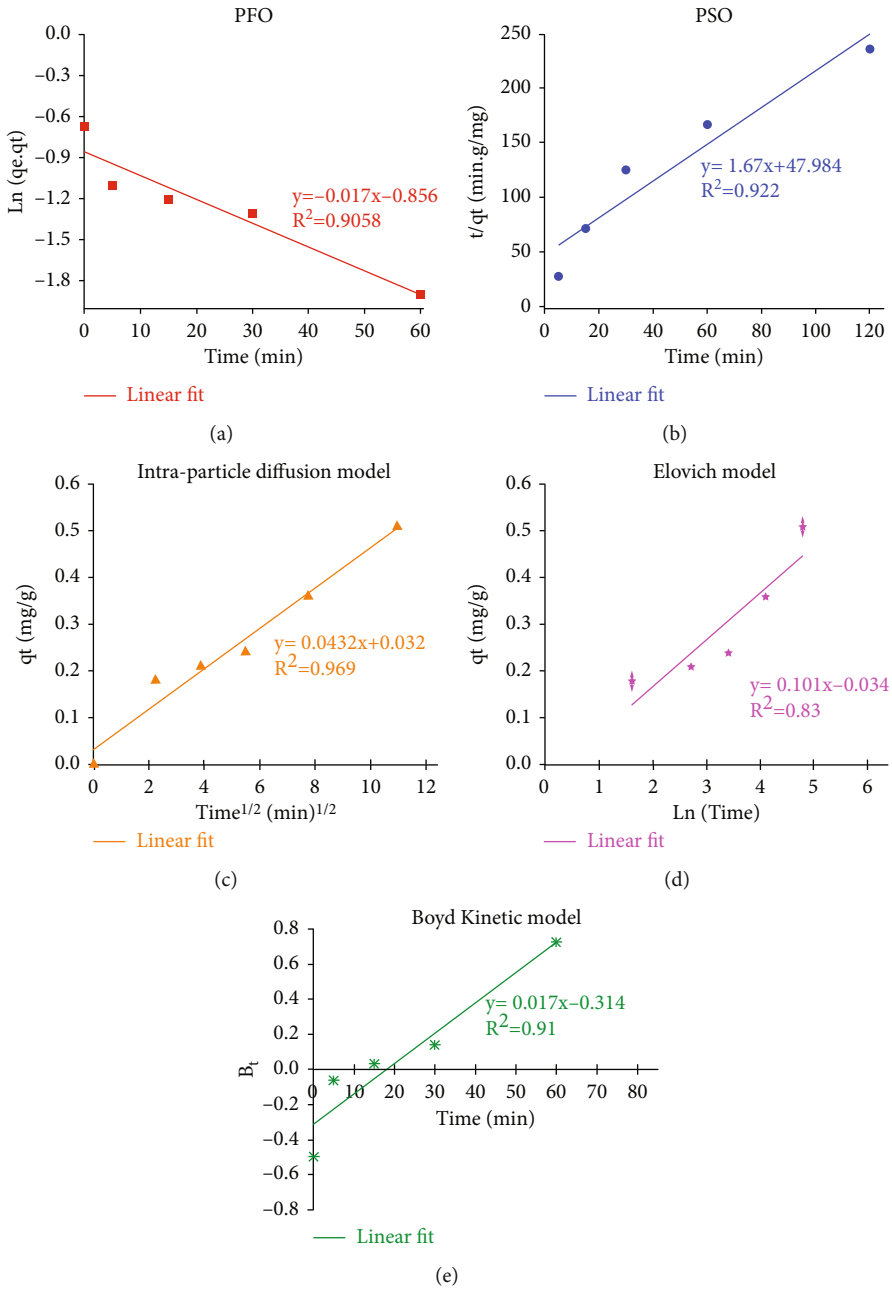

Figure 5: Kinetic studies: (a) pseudo-first-order (PFO), (b) pseudo-second-order (PSO), (c) intraparticle diffusion, (d) Elovich, and (e) Boyd kinetic models.

process on the exterior surface of the adsorbent at the initial stage while at the later stages, dominating most of the exterior sites, the adsorbate molecules could start penetrating the pores to reach the interior adsorption sites at a slow process.

3.4. Kinetic Studies. The linearized forms of the pseudo-first-order (PFO), pseudo-second-order (PSO), intraparticle diffusion, and Elovich and Boyd kinetic models are depicted in Figure 5. Generally, a good fit of the experimental data to the different models was observed. The results illustrate that the correlation coefficient (R^2) corresponding to PSO was the highest value at 0.9217. Thus, the adsorption of phenol onto aluminum oxide nanoparticles demonstrated the best fit with the PSO model. Thus, chemisorption can be considered the rate-limiting step because the process of adsorption involves exchanging or sharing electrons between phenol and the aluminum oxide nanoparticles according to the assumption of PSO [51]. The values of q_e and k_2 were 0.595 mg/g and 0.0588 g/mg·min.

Because the three kinetic models cannot describe the mechanism of diffusion, additional models were tested to determine the rate-controlling steps in the phenol adsorption. During the phenol uptake, three successive steps can

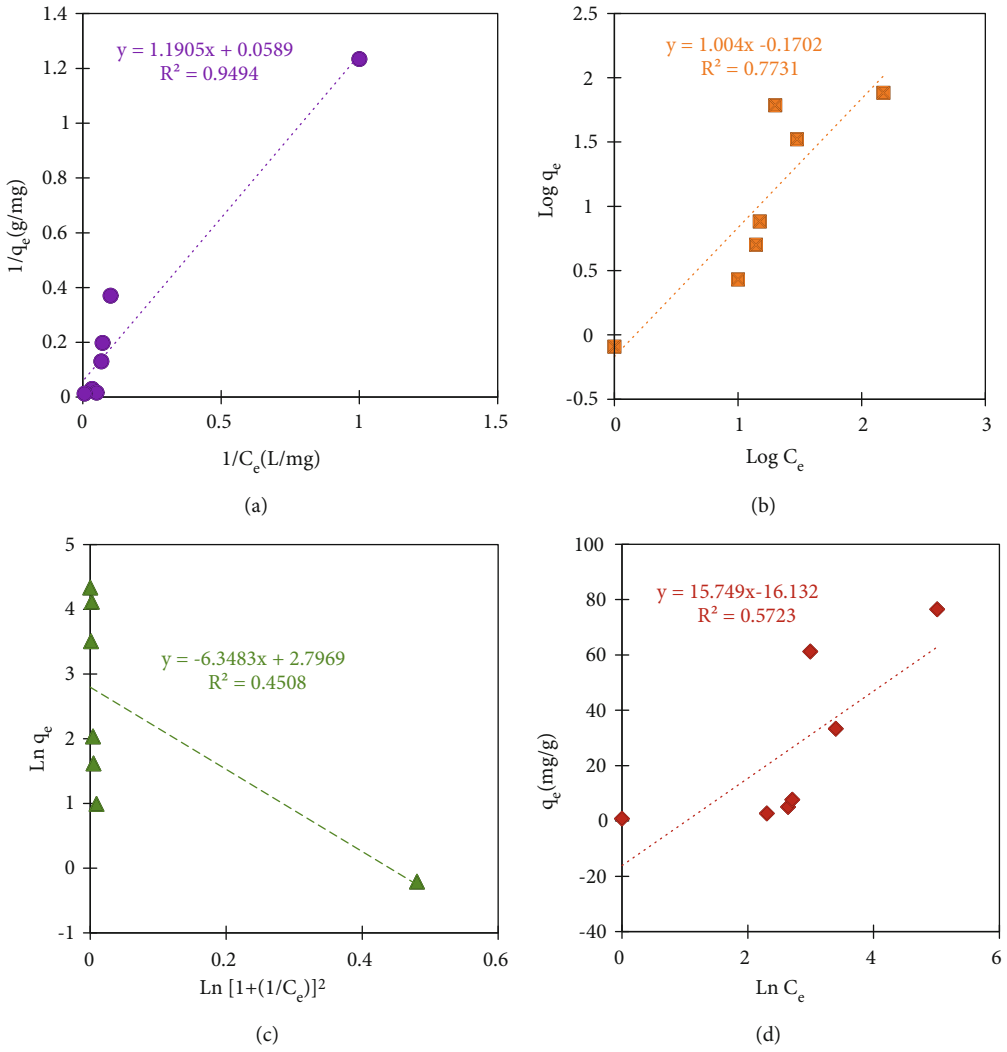

Figure 6: Isotherms: (a) Langmuir, (b) Freundlich, (c) Dubinin-Radushkevich, and (d) Temkin.

Table 1: Comparison of the maximum capacities of the adsorption of phenol onto different materials.

Adsorbent material	Maximum capacity of adsorption (mg/g)	Reference
Granular activated carbon	75.5	[53]
Natural coal	18.8	[54]
Bentonite	0.52	[10]
Aluminum oxide	0.35	[34]
Red mud	4.13	[55]
Aluminum oxide nanoparticles	16.97	This study

occur. First, phenol transfers from the bulk solution to the external surface of the nanoparticles in a step called film diffusion. Second, phenol moves through the interior particles of the nanoparticles in a step called particle diffusion. Third, phenol attaches to the interior surface of the nanoparticles in a step called adsorption. Figure 5(c) shows the linear form of the data using the intraparticle diffusion model. Because the data can be divided into three linear portions, the process of adsorption is controlled through a multistep mechanism. The value of K_P was 0.0432 mg/g·min$^{0.5}$. The linear form of the Boyd kinetic model is displayed in Figure 5(d) and was used to distinguish between the film diffusion and particle diffusion. Because the fitting line for the data does not pass through the origin, the process of adsorption of phenol onto aluminum oxide nanoparticles is controlled by film diffusion.

3.5. Equilibrium Studies. Four different isotherms were examined to find the appropriate model for the design process. Each isotherm has certain assumptions. In the Langmuir isotherm, all sites of adsorption have the same energy. In the Freundlich isotherm, the adsorption occurs on a heterogeneous surface. In the Dubinin-Radushkevich isotherm, it interprets the porous structure of the surface of the nanoparticles. In the Temkin isotherm, a linear decrease in the heat of the adsorption occurs along with the coverage of the surface. Figures 6(a)–6(d) reveal the

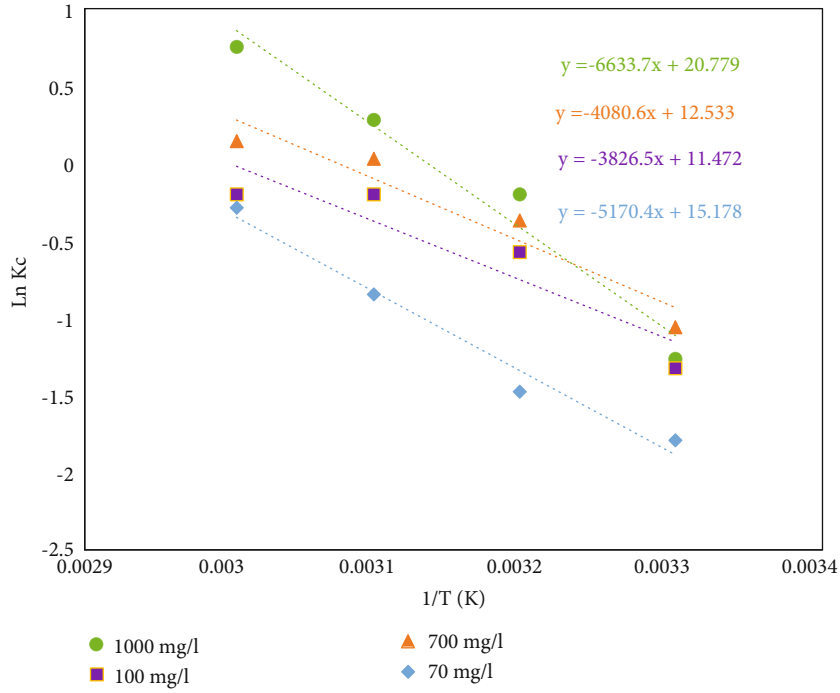

Figure 7: Linear plots of data for the thermodynamic model.

Table 2: Thermodynamic model parameters.

Initial Conc. (mg/L)	ΔH° (kJ/Mol)	ΔS° (J/Mol/K)	ΔG° (kJ/Mol)			
			30°C	40°C	50°C	60°C
1000	55.15	172.76	2.8	1.07	−0.66	−2.38
700	33.92	104.17	2.36	1.31	0.27	−0.77
100	31.81	95.36	2.91	1.96	1.01	0.05
70	42.98	126.21	4.74	3.48	2.22	0.96

linear plots of the four isotherms. The results demonstrate that the maximum coefficient of correlation was obtained using the Langmuir isotherm ($R^2 = 0.9494$). Thus, the equilibrium data were best represented by the Langmuir isotherm and the surface of the aluminum oxide nanoparticles was homogenous with identical sites where the monolayer adsorption occurred [52]. The maximum capacity of adsorption was 16.97 mg/g, while the value of K_L was 0.049 mg/L. For the Freundlich isotherm, the values of n and K_F were 1.004 and 0.675 mg/g $(\text{mg/L})^{1.004}$, respectively. For the Dubinin-Radushkevich isotherm, the value of q_{DR} was 16.39 mg/g. For the Temkin isotherm, the values of B_1 and K_T were 15.749 and 0.359 mg/L, respectively. The standard deviations between the best two isotherm models (Langmuir versus Freundlich) were considered, and the statistical analysis with t-test revealed that the standard error and standard deviation for Langmuir were the lowest value (i.e., standard deviation: 0.36 vs 0.65). In terms of the p value, there was no significant difference in the two models at 95% significance level (p value > 0.05). Table 1 reveals the value of the maximum capacity of the adsorption of phenol onto different types of adsorbents. It is obvious that the performance of nanoparticles was better than that of the normal aluminum oxide with respect to the maximum adsorption capacity. However, other adsorbents, including granular-activated carbon and natural coal, have higher adsorption capacity.

The removal efficiencies of phenol, using aluminum oxide nanoparticles, are higher than those obtained when using adsorbents with a large particle size and are quite similar to those obtained from some other nanoparticles. For example, vernadite was used for the removal of phenol, through the adsorption process, and the maximum removal efficiency was approximately 85% [56]. On the other hand, phenol removal was examined using nano-zero-valent iron and supported nano-zero-valent iron and the removal efficiencies were approximately 94% and 90%, respectively, which is close to the values obtained in this study [57]. When the phenol removal efficiencies are compared with those of other treatment technologies, the adsorption process using nanoparticles shows excellent results. In a study using the electrocoagulation technique with zinc electrodes, the maximum efficiency of phenol removal was 85% [58]. In another study, microbial fuel cells were used to remove phenol and the maximum removal efficiency reached was 63% [59]. Therefore, the use of aluminum oxide nanoparticles for phenol removal is better than the use of other treatment technologies, not only because there is high removal efficiency but also because other systems are more complex. Moreover, metal oxide adsorbents can provide an additional benefit, since adsorbents can be used, after the adsorption process, in a photocatalytic oxidation reactor where further removal of phenol can be achieved [60].

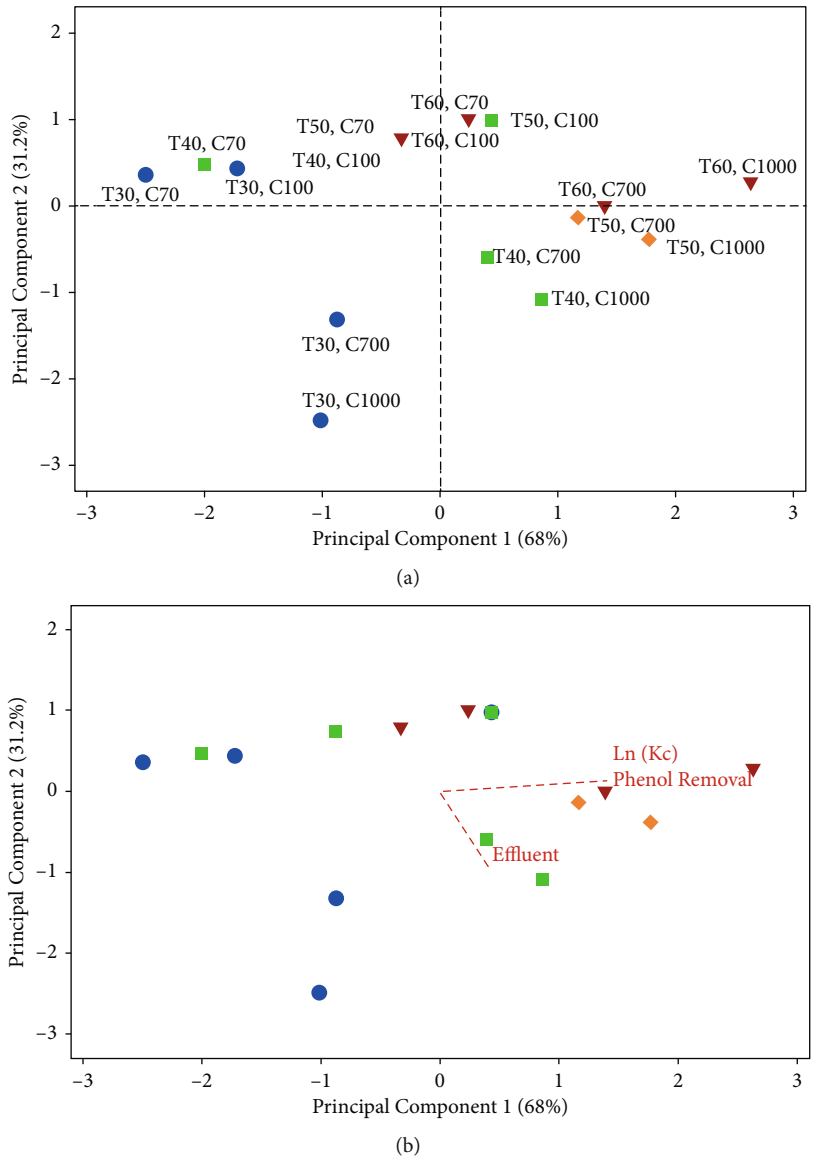

FIGURE 8: (a) Score plot for PCA analysis of treated samples, PC 1 (68%) and PC 2 (31.2%). (b) Biplot and loading plot of PC1 and PC2 with project lines of all treated samples where sample loadings are represented as vectors radiating from the origin. Sample scores are color coded and indicated by symbols according to each temperature; samples that are similar will plot near to each other (clustered together).

3.6. Thermodynamics. Figure 7 reveals the linear plot of the thermodynamic equation (ln Kc versus $1/T$). Table 2 lists the values of Gibbs-free energy, entropy, and enthalpy at various concentrations and temperatures. The results indicate that the process of adsorption is endothermic due to the positive sign of ΔH°, indicating that a high amount of heat is used to transfer the phenol from the solution to the nanoparticles [61]. At low temperatures, the phenol uptake is nonspontaneous due to the positive sign of ΔG°, while at high concentrations and high temperatures, the phenol uptake was spontaneous. Some structural changes occurred as shown by the positive sign of ΔS°.

The principal component analysis (PCA) was performed to further reveal the relative influence of aluminum oxide nanoparticles on adsorption and various adsorption parameters (Figure 8). The respective contribution to the total variance in PCA analysis of all treated samples was manifested by varying percentages of 68 and 31.2 for both axes PC 1 and PC 2, respectively. The variations in the PC1 direction contributed to 68% of the total variations, and this attributes to the broad separation of the adsorption-treated samples in this direction. The data for high temperatures (50 and 60°C) and high concentration samples (700 and 1000 mg/L) denoted as (T60, C1000; T60, C700; T50, C1000; and T50, C700) were clustered together in the right quadrants. The temperature at 60°C only (T60, C700 and T60, C1000) was singled out in the top-right quadrant. For the low concentrations and low-temperature treatment (T30, C70; T30, C100; T40, C70; and T40, C100), the samples were associated in few groups and clusters directed to the opposite direction of PC1.

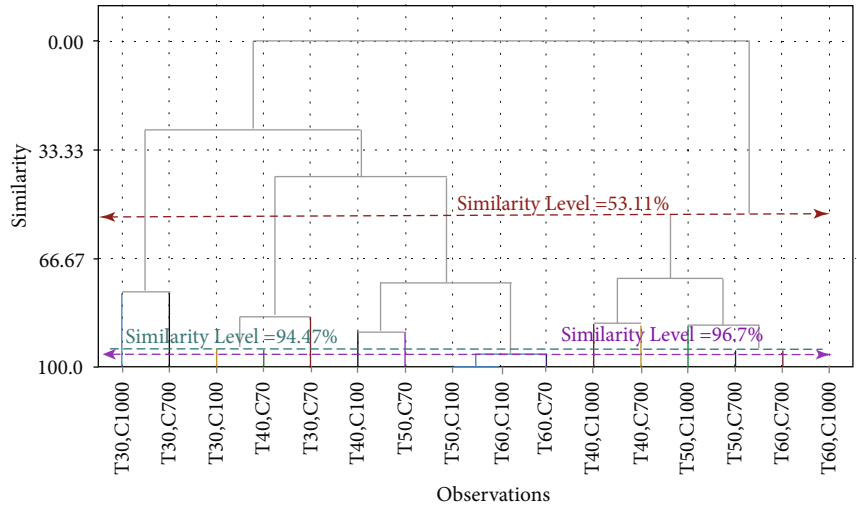

Figure 9: Dendrogram of the cluster analysis for all treated samples based on adsorption conditions. At a similarity level of 51.1, 4 main clusters were observed similar to PCA.

Table 3: Desorption efficiencies at various HCl concentrations at the initial concentration of phenol of 400 mg/L.

HCl concentration (N)	Desorption efficiency (%)
0.1	43.75
0.2	45
0.4	46.25
0.6	46.75
0.8	50
1	50.25

Generally, group 1 and group 2 samples exhibited a weak association with phenol removal and ln (Kc) loading vectors where the phenol removal and ln (Kc) peaks were positively shifted towards the left-bottom and top quadrants. The PCA emphasize this decrease in phenol removal and rate of removal as observed in the positive values of ΔG° (Table 2). This matches the negative scores of those conditions on PC1 and their relative positions in the same part with high temperatures and high concentrations. In contrast, group 3 and 4 samples were considerably varied and mostly grouped in the top-right quadrants. Notably, the group 3 and 4 samples were intensified in the direction vectors of effluent, phenol removal, and rate of adsorption, demonstrating the outperformance of T50 and T60 at high concentrations in adsorption.

In the same sense, a cluster analysis was performed to examine the influence of aluminum oxide nanoparticles on adsorption and correlate it with the PCA observations (Figure 9). Similarly, the cluster analysis emphasized four main clusters of data at a similar level of 53.11 in which cluster 1 encompassed (T30, C100; T30, C70; and T40, C70); cluster 2 included (T30, C1000 and T30, C700); cluster 3 included (T60, C100; T50, C100; T40, C100; and T50, C70); and cluster 4 encompassed (T60, C1000; T60, C700; T50, C1000; T50, C700; T40, C1000; and T40, C700). The results indicated that metrics based on concentration and adsorption temperatures are favorable for multivariate analysis and PCA assessment to categorize adsorption conditions based on their relative performances.

3.7. Regeneration of the Nanoparticles. It is important to study the regeneration ability of the consumed adsorbent to reduce the cost of the process of adsorption and to decrease the problems associated with the disposal of the consumed material [30]. In practice, regeneration studies have been performed using solvents, such as acids. Hydrochloric acid (HCl) has been used for desorption experiments, and various concentrations have been used ranging from 0.2 to 1 N HCl. Table 3 displays the desorption efficiencies at various HCl concentrations. The results demonstrated that HCl could remove up to 50% of the amount of the phenol on the nanoparticle surface and an approximately constant value of removal was reached at 0.8 N HCl and higher.

4. Conclusion

Aluminum oxide nanoparticles successfully exhibited superior phenol removal from an aqueous solution in addition to a high potential regeneration of the consumed nanoparticles by HCl. The nanoparticles were crystalline in nature due to the existence of peaks. At higher pH values, the removal efficiencies were lower than those obtained at low pH values. The maximum removal efficiency of phenol reached 92.5% in which an increasing trend of efficiency was observed with the increase of the dose. The results reveal that the efficiency of the removal of phenol increased with increased stirring speeds. Kinetic studies showed that the data fit the PSO kinetic model. The adsorption of phenol onto aluminum oxide nanoparticles is controlled by film diffusion. Based on the equilibrium experiments, the data demonstrated the best fit with the Langmuir isotherm. The results indicated that the process of adsorption is endothermic due to the positive sign of ΔH°. At low temperatures, the phenol uptake is nonspontaneous due to the positive sign of ΔG°, while at

high concentrations and high temperatures, the phenol uptake was spontaneous. The relative differences demonstrated for adsorption processes in terms of endothermic and spontaneity were confirmed by PCA. This evidence is key for future investigations of the efficiency of adsorption conditions concerning the contaminant type and adsorbate compounds. In a real system, alumina nanoparticles can be used in a fixed bed column and their application performance can be enhanced through the support of the nanoparticles onto another larger-scale material. Given the proof of concept presented here and our investigations, the knowledge gap highlights the need for further studies to be warranted to progress the work in this area and the practical aspects of these methods and the effects of other parameters for real applications.

Data Availability

All the data used to support the findings of this study are included within the article.

Disclosure

This research did not receive any specific grant from funding agencies in the public, commercial, or not-for-profit sectors.

Conflicts of Interest

The authors declare that they have no conflicts of interest.

References

[1] F. E. Bulletin, M. Sciences, and M. Sciences, "Phenol removal by electrocoagulation process from aqueous solutions," *Fresenius Environmental Bulletin*, vol. 21, no. 2, pp. 364–371, 2012.

[2] A. Almasi, A. Dargahi, A. Amrane, M. Fazlzadeh, M. Mahmoudi, and A. Hashemian, "Effect of the retention time and the phenol concentration on the stabilization pond efficiency in the treatment of oil refinery wastewater," *Fresenius Environmental Bulletin*, vol. 23, no. 10A, pp. 2541–2548, 2014.

[3] N. V. Pradeep, S. Anupama, K. Navya, H. N. Shalini, M. Idris, and U. S. Hampannavar, "Biological removal of phenol from wastewaters: a mini review," *Applied Water Science*, vol. 5, no. 2, pp. 105–112, 2015.

[4] A. Abu-Nada, A. Abdala, and G. McKay, "Removal of phenols and dyes from aqueous solutions using graphene and graphene composite adsorption: a review," *Journal of Environmental Chemical Engineering*, vol. 9, no. 5, article 105858, 2021.

[5] M. Mamdouh, S. M. Safwat, H. Abd-Elhalim, and E. Rozaik, "Urea removal using electrocoagulation process with copper and iron electrodes," *Desalination and Water Treatment*, vol. 213, pp. 259–268, 2021.

[6] O. A. Shaker, M. E. Matta, and S. M. Safwat, "Nickel and chromium removal by electrocoagulation using copper electrodes," *Desalination and Water Treatment*, vol. 213, pp. 371–380, 2021.

[7] J. D. Muñoz Sierra, M. J. Oosterkamp, W. Wang, H. Spanjers, and J. B. van Lier, "Impact of long-term salinity exposure in anaerobic membrane bioreactors treating phenolic wastewater: performance robustness and endured microbial community," *Water Research*, vol. 141, pp. 172–184, 2018.

[8] H. Luo, G. Liu, R. Zhang, and S. Jin, "Phenol degradation in microbial fuel cells," *Chemical Engineering Journal*, vol. 147, no. 2–3, pp. 259–264, 2009.

[9] S. M. Safwat and M. E. Matta, "Adsorption of urea onto granular activated alumina: a comparative study with granular activated carbon," *Journal of Dispersion Science and Technology*, vol. 39, no. 12, pp. 1699–1709, 2018.

[10] S. M. Safwat, M. Medhat, and H. Abdel-Halim, "Phenol adsorption onto kaolin and fuller's earth: a comparative study with bentonite," *Desalination and Water Treatment*, vol. 155, pp. 197–206, 2019.

[11] J. Pei, Z. Chen, Y. Wang et al., "Preparation of phosphorylated iron-doped ZIF-8 and their adsorption application for U (VI)," *Journal of Solid State Chemistry*, vol. 305, 2022.

[12] B. Hayati and N. M. Mahmoodi, "Modification of activated carbon by the alkaline treatment to remove the dyes from wastewater: mechanism, isotherm and kinetic," *Desalination and Water Treatment*, vol. 47, no. 1–3, pp. 322–333, 2012.

[13] S. H. Lin and R. S. Juang, "Adsorption of phenol and its derivatives from water using synthetic resins and low-cost natural adsorbents: a review," *Journal of Environmental Management*, vol. 90, no. 3, pp. 1336–1349, 2009.

[14] S. Chang, W. Xie, C. Yao et al., "Construction of 2D porphyrin-based covalent organic framework as adsorbent for organic dyes removal and carbon dioxide adsorption," *Journal of Solid State Chemistry*, vol. 304, article 122577, 2021.

[15] N. M. Mahmoodi, M. Taghizadeh, and A. Taghizadeh, "Activated carbon/metal-organic framework composite as a bio-based novel green adsorbent: preparation and mathematical pollutant removal modeling," *Journal of Molecular Liquids*, vol. 277, pp. 310–322, 2019.

[16] S. M. Safwat, "Performance evaluation of paroxetine adsorption using various types of activated carbon," *International Journal of Civil Engineering*, vol. 17, no. 10, pp. 1619–1629, 2019.

[17] S. Noreen, H. N. Bhatti, M. Iqbal, F. Hussain, and F. M. Sarim, "Chitosan, starch, polyaniline and polypyrrole biocomposite with sugarcane bagasse for the efficient removal of acid black dye," *International Journal of Biological Macromolecules*, vol. 147, pp. 439–452, 2020.

[18] H. N. Bhatti, Y. Safa, S. M. Yakout, O. H. Shair, M. Iqbal, and A. Nazir, "Efficient removal of dyes using carboxymethyl cellulose/alginate/polyvinyl alcohol/rice husk composite: adsorption/desorption, kinetics and recycling studies," *International Journal of Biological Macromolecules*, vol. 150, pp. 861–870, 2020.

[19] S. A. Hosseini, M. Vossoughi, N. M. Mahmoodi, and M. Sadrzadeh, "Efficient dye removal from aqueous solution by high-performance electrospun nanofibrous membranes through incorporation of SiO2 nanoparticles," *Journal of Cleaner Production*, vol. 183, pp. 1197–1206, 2018.

[20] U. Kamran, H. N. Bhatti, M. Iqbal, S. Jamil, and M. Zahid, "Biogenic synthesis, characterization and investigation of photocatalytic and antimicrobial activity of manganese nanoparticles synthesized from Cinnamomum verum bark extract," *Journal of Molecular Structure*, vol. 1179, pp. 532–539, 2019.

[21] A. Stafiej and K. Pyrzynska, "Adsorption of heavy metal ions with carbon nanotubes," *Separation and Purification Technology*, vol. 58, no. 1, pp. 49–52, 2007.

[22] B. S. Tawabini, S. F. Al-Khaldi, M. M. Khaled, and M. A. Atieh, "Removal of arsenic from water by iron oxide nanoparticles impregnated on carbon nanotubes," *Journal of Environmental Science and Health-Part A Toxic/Hazardous Substances and Environmental Engineering*, vol. 46, no. 3, pp. 215–223, 2011.

[23] A. Goswami, P. K. Raul, and M. K. Purkait, "Arsenic adsorption using copper (II) oxide nanoparticles," *Chemical Engineering Research and Design*, vol. 90, no. 9, pp. 1387–1396, 2012.

[24] Y. Ma, Y. M. Zheng, and J. P. Chen, "A zirconium based nanoparticle for significantly enhanced adsorption of arsenate: synthesis, characterization and performance,," *Journal of Colloid and Interface Science*, vol. 354, no. 2, pp. 785–792, 2011.

[25] C. Sakulthaew, C. Chokejaroenrat, A. Poapolathep, T. Satapanajaru, and S. Poapolathep, "Hexavalent chromium adsorption from aqueous solution using carbon nano-onions (CNOs)," *Chemosphere*, vol. 184, pp. 1168–1174, 2017.

[26] Z. Ghasemi, A. Seif, T. S. Ahmadi, B. Zargar, F. Rashidi, and G. M. Rouzbahani, "Thermodynamic and kinetic studies for the adsorption of Hg (II) by nano-TiO 2 from aqueous solution," *Advanced Powder Technology*, vol. 23, no. 2, pp. 148–156, 2012.

[27] S. Banerjee, S. Dubey, R. K. Gautam, M. C. Chattopadhyaya, and Y. C. Sharma, "Adsorption characteristics of alumina nanoparticles for the removal of hazardous dye, orange G from aqueous solutions," *Arabian Journal of Chemistry*, vol. 12, no. 8, pp. 5339–5354, 2019.

[28] S. Tabesh, F. Davar, and M. R. Loghman-Estarki, "Preparation of γ-Al2O3 nanoparticles using modified sol-gel method and its use for the adsorption of lead and cadmium ions," *Journal of Alloys and Compounds*, vol. 730, pp. 441–449, 2018.

[29] P. Jeevanandam, K. J. Klabunde, and S. H. Tetzler, "Adsorption of thiophenes out of hydrocarbons using metal impregnated nanocrystalline aluminum oxide," *Microporous and Mesoporous Materials*, vol. 79, no. 1–3, pp. 101–110, 2005.

[30] S. Banerjee, R. K. Gautam, A. Jaiswal, M. C. Chattopadhyaya, and Y. C. Sharma, "Rapid scavenging of methylene blue dye from a liquid phase by adsorption on alumina nanoparticles," *RSC Advances*, vol. 5, no. 19, pp. 14425–14440, 2015.

[31] L. Liu, Z. Cui, Q. Ma, W. Cui, and X. Zhang, "One-step synthesis of magnetic iron-aluminum oxide/graphene oxide nanoparticles as a selective adsorbent for fluoride removal from aqueous solution," *RSC Advances*, vol. 6, no. 13, pp. 10783–10791, 2016.

[32] C. Liu, Z. Chen, C. Ni et al., "Adsorption of phenol from aqueous solution by a hierarchical micro-nano porous carbon material," *Rare Metals*, vol. 31, no. 6, pp. 582–589, 2012.

[33] Y. H. Kim, B. Lee, K. H. Choo, and S. J. Choi, "Adsorption characteristics of phenolic and amino organic compounds on nano-structured silicas functionalized with phenyl groups," *Microporous and Mesoporous Materials*, vol. 185, pp. 121–129, 2014.

[34] S. M. Safwat, M. Medhat, and H. Abdel-Halim, "Adsorption of phenol onto aluminium oxide and zinc oxide: a comparative study with titanium dioxide," *Separation Science and Technology (Philadelphia)*, vol. 54, no. 17, pp. 2840–2852, 2019.

[35] X. Wang, "Nanomaterials as sorbents to remove heavy metal ions in wastewater treatment," *Journal of Environmental & Analytical Toxicology*, vol. 2, no. 7, 2012.

[36] M. Habuda-Stanić and M. Nujić, "Arsenic removal by nanoparticles: a review," *Environmental Science and Pollution Research*, vol. 22, no. 11, pp. 8094–8123, 2015.

[37] A. S. Jbara, Z. Othaman, A. A. Ati, and M. A. Saeed, "Characterization of γ- Al2O3 nanopowders synthesized by co-precipitation method," *Materials Chemistry and Physics*, vol. 188, pp. 24–29, 2017.

[38] A. D. Rice, E. W. Baird, and R. B. Eaton, *Standard Methods for the Examination of Water and Wastewater*, American Public Health Association, Washington DC, 23rd edition, 2017.

[39] N. M. Mahmoodi, M. Taghizadeh, and A. Taghizadeh, "Mesoporous activated carbons of low-cost agricultural bio-wastes with high adsorption capacity: preparation and artificial neural network modeling of dye removal from single and multicomponent (binary and ternary) systems," *Journal of Molecular Liquids*, vol. 269, pp. 217–228, 2018.

[40] S. M. Safwat, A. Ali, and M. E. Matta, "Adsorption of copper using fuller's earth: kinetics, equilibrium and thermodynamics," *Journal of Engineering and Applied Science*, vol. 67, no. 7, pp. 1729–1746, 2020.

[41] M. N. A. Meshref, S. M. M. Azizi, W. Dastyar, R. Maal-Bared, and B. R. Dhar, "Low-temperature thermal hydrolysis of sludge prior to anaerobic digestion: Principal component analysis (PCA) of experimental data," *Data in Brief*, vol. 38, article 107323, 2021.

[42] R. Prabhakar and S. R. Samadder, "Low cost and easy synthesis of aluminium oxide nanoparticles for arsenite removal from groundwater: a complete batch study," *Journal of Molecular Liquids*, vol. 250, pp. 192–201, 2018.

[43] P. C. C. Faria, J. J. M. Órfão, and M. F. R. Pereira, "Adsorption of anionic and cationic dyes on activated carbons with different surface chemistries," *Water Research*, vol. 38, no. 8, pp. 2043–2052, 2004.

[44] V. Nair, A. Panigrahy, and R. Vinu, "Development of novel chitosan-lignin composites for adsorption of dyes and metal ions from wastewater," *Chemical Engineering Journal*, vol. 254, pp. 491–502, 2014.

[45] S. Nethaji, A. Sivasamy, G. Thennarasu, and S. Saravanan, "Adsorption of malachite green dye onto activated carbon derived from Borassus aethiopum flower biomass," *Journal of Hazardous Materials*, vol. 181, no. 1–3, pp. 271–280, 2010.

[46] T. Viraraghavan and F. De Maria Alfaro, "Adsorption of phenol from wastewater by peat, fly ash and bentonite," *Journal of Hazardous Materials*, vol. 57, no. 1–3, pp. 59–70, 1998.

[47] G. Dursun, H. Çiçek, and A. Y. Dursun, "Adsorption of phenol from aqueous solution by using carbonised beet pulp," *Journal of Hazardous Materials*, vol. 125, no. 1–3, pp. 175–182, 2005.

[48] I. A. W. Tan, A. L. Ahmad, and B. H. Hameed, "Adsorption isotherms, kinetics, thermodynamics and desorption studies of 2, 4, 6-trichlorophenol on oil palm empty fruit bunch-based activated carbon," *Journal of Hazardous Materials*, vol. 164, no. 2–3, pp. 473–482, 2009.

[49] Y. H. Magdy and H. Altaher, "Kinetic analysis of the adsorption of dyes from high strength wastewater on cement kiln dust," *Journal of Environmental Chemical Engineering*, vol. 6, no. 1, pp. 834–841, 2018.

[50] J. Huang, X. Wang, Q. Jin, Y. Liu, and Y. Wang, "Removal of phenol from aqueous solution by adsorption onto OTMAC-modified attapulgite," *Journal of Environmental Management*, vol. 84, no. 2, pp. 229–236, 2007.

[51] M. Basu, A. K. Guha, and L. Ray, "Adsorption of lead on cucumber peel," *Journal of Cleaner Production*, vol. 151, pp. 603–615, 2017.

[52] H. Kaur, A. Bansiwal, G. Hippargi, and G. R. Pophali, "Effect of hydrophobicity of pharmaceuticals and personal care products for adsorption on activated carbon: adsorption isotherms, kinetics and mechanism," *Environmental Science and Pollution Research*, vol. 25, no. 21, pp. 20473–20485, 2018.

[53] C. C. Leng and N. G. Pinto, "Effects of surface properties of activated carbons on adsorption behavior of selected aromatics," *Carbon*, vol. 35, no. 9, pp. 1375–1385, 1997.

[54] Y. I. Tarasevich, "Porous structure and adsorption properties of natural porous coal," *Colloids and Surfaces A: Physicochemical and Engineering Aspects*, vol. 176, no. 2–3, pp. 267–272, 2001.

[55] V. K. Gupta, S. Sharma, I. S. Yadav, and D. Mohan, "Utilization of bagasse fly ash generated in the sugar industry for the removal and recovery of phenol and *p*-nitrophenol from wastewater," *Journal of Chemical Technology and Biotechnology*, vol. 71, no. 2, pp. 180–186, 1998.

[56] B. Wang, N. Ouyang, Q. Zhang et al., "Study on the removal performance of phenol and lead by vernadite synthesized via a new method," *Adsorption Science and Technology*, vol. 2021, 2021.

[57] S. T. Kadhum, G. Y. Alkindi, and T. M. Albayati, "Eco friendly adsorbents for removal of phenol from aqueous solution employing nanoparticle zero-valent iron synthesized from modified green tea bio-waste and supported on silty clay," *Chinese Journal of Chemical Engineering*, vol. 36, pp. 19–28, 2021.

[58] A. S. Fajardo, R. F. Rodrigues, R. C. Martins, L. M. Castro, and R. M. Quinta-Ferreira, "Phenolic wastewaters treatment by electrocoagulation process using Zn anode," *Chemical Engineering Journal*, vol. 275, pp. 331–341, 2015.

[59] S. M. Safwat, E. Rozaik, and H. Abdel-Halim, "A comparative study on treatment of wastewaters with various biodegradability and various pH values using single-chamber microbial fuel cells," *Water and Environment Journal*, vol. 33, no. 3, pp. 409–417, 2019.

[60] L. Yu, X. Peng, F. Ni, J. Li, D. Wang, and Z. Luan, "Arsenite removal from aqueous solutions by γ-Fe2O3-TiO2 magnetic nanoparticles through simultaneous photocatalytic oxidation and adsorption," *Journal of Hazardous Materials*, vol. 246, pp. 10–17, 2013.

[61] A. R. Kul and H. Koyuncu, "Adsorption of Pb (II) ions from aqueous solution by native and activated bentonite: kinetic, equilibrium and thermodynamic study," *Journal of Hazardous Materials*, vol. 179, no. 1–3, pp. 332–339, 2010.